Reprinted from the Journal of the American Ceramic Society, Vol. 75, No. 3, March 1992

Densification of Reaction-Synthesized Titanium Carbide by High-Velocity Forging

Jerry C. LaSalvia, Lothar W. Meyer, and Marc A. Meyers

journal

J. Am. Ceram. Soc., 75 [3] 592–602 (1992)

Densification of Reaction-Synthesized Titanium Carbide by High-Velocity Forging

Jerry C. LaSalvia, Lothar W. Meyer,* and Marc A. Meyers

Department of Applied Mechanics and Engineering Sciences, University of California—San Diego, La Jolla, California 92093

A novel process for the manufacture of dense titanium carbide is described. Titanium carbide is produced by the reaction synthesis method, while densification and near-net shaping is accomplished by a high-velocity forging step. Disks with 10-cm diameter were produced with densities over 96% of the theoretical density. The major problem encountered in this study has been thermal shock. Use of insulation and furnace cooling has decreased the severity of this problem. Optical and scanning electron microscopy observations of the resulting microstructure reveal equiaxed grains with an average size of 44 μm. Quasi-static and high-strain-rate compressive strength measurements yield values greater than 1.7 and 2.2 GPa, respectively. The morphologies of thermally induced (slow) and rapidly propagating cracks were characterized and the fracture modes were found to be intergranular and transgranular, respectively. The addition of Ni (5 and 25 wt%) yielded a ceramic–metal composite with a favorable microstructure. [Key words: titanium carbide, combustion synthesis, forging, thermal shock, strength.]

I. Introduction

REACTION synthesis, also commonly referred to as self-propagating high-temperature synthesis (SHS) or combustion synthesis, is a materials processing technique by which monolithic ceramics, ceramic-matrix composites, and intermetallic compounds can be produced. Taking the classic thermite (exothermic) reaction as an example of the process, $Fe_2O_3 + 2Al \rightarrow Al_2O_3 + 2Fe$, iron oxide powder is mixed with aluminum powder. In order for the reaction to occur, energy must be initially supplied to overcome the activation energy barrier for the reaction. The amount of energy supplied has to be sufficient to convert a fraction of the reactants to the final product(s). The subsequent energy release by the conversion of the reactants to the final product is sufficiently large to continuously propagate the reaction in the surrounding mixture. The reaction continues until all of the reactants have been consumed, hence the term self-propagating. Examples of materials that have been produced by this method include carbides, borides, cemented carbides, ceramic-matrix composites, intermetallics, nitrides, and hydrides.[1]

The Soviet Union has by far the most developed SHS research program, which was initiated in 1967 by Merzhanov.[2] It has been estimated that researchers in the Soviet Union have synthesized over 300 (conservative value) different materials by this method, with many being produced on an industrial level.[3] Reviews on SHS have been made by Frankhouser *et al.*,[4] Munir and Anselmi-Tamburini,[5] Hardt,[6] McCauley,[7] Holt,[8] and Merzhanov.[9]

Fig. 1 is a scanning electron micrograph of a reaction-synthesized titanium carbide microstructure obtained in this study. The lighter regions are titanium carbide, while the darker regions are voids. As can be seen from this micrograph, the porosity is approximately 50%. This final porosity results from the initial green body porosity, the lower specific volume of the final product compared to the reactants, and the volatilization of impurities. The porosity represents the failure of liquid-phase (transient) sintering mechanisms to successfully densify the body.[10]

A number of techniques are being studied or employed to densify the final product. In the Soviet Union, these techniques include hot-pressing, extrusion, and explosive compaction.[11] In Japan, pressure-assisted reactive sintering (RHIP) is being studied.[12–15] In the United States, pressureless reactive sintering,[16,17] pressure-assisted reactive sintering (RHIP),[18] hot-pressing,[19–21] rolling,[22] and explosive compaction[23–25] are being investigated.

This report describes a new densification technique which has been applied to reaction-synthesized titanium carbide (Hoke *et al.*[26] are studying the application of this technique to reaction-synthesized titanium diboride). This technique uses a high-velocity forging machine which has traditionally been used for hot-working metal alloys. An important criterion that the material being forged must meet is the ability to flow plastically (possibly large plastic deformations) without failure. Ceramics usually do not exhibit any significant bulk plasticity due to the nature of their atomic bonding. However, if they are raised to a high enough temperature, plastic deformation is possible. Indeed, for titanium carbide, this brittle-to-ductile transition occurs somewhere between 800° and 1200°C.[27–29] Experimental temperature measurements of the reaction producing titanium carbide yield values much greater than 1200°C.[23] Adiabatic temperature calculations predict a peak temperature of 3060°C (melting point of TiC) with 33% of the product melted.[20] Therefore, it seems plausible that the forging technique can be used in conjunction with reaction synthesis to produce fully dense titanium carbide.

II. Experimental Procedure

The powders used in this study consisted of elemental titanium (Micron Metals Inc., Salt Lake City, UT), nickel (Aldrich Chemical Co., Milwaukee, WI), and carbon (in the form of graphite; Consolidated Astronautics, Smithtown, NY). The particle sizes for the titanium, nickel, and carbon powders were 44 (325 mesh), 3, and 2 μm, respectively. The titanium and carbon powders (i.e., manufacturers and size) were chosen on the basis of earlier research conducted by Niiler and co-workers[23] on the reaction synthesis of titanium carbide and titanium diboride.

R.W. Rice—contributing editor

Manuscript No. 196728. Received May 2, 1991; approved November 4, 1991.
Presented at the 92nd Annual Meeting of the American Ceramic Society, April 23, 1990 (Engineering Ceramics Division, Paper No. 28-C-90).
Supported by the Army Research Office under Contract No. ARO-DAAL-03-88-K-0194.
*Fraunhofer Institut fur Angewandte Materialsforchung, D-282 Bremen 77, Federal Republic of Germany.

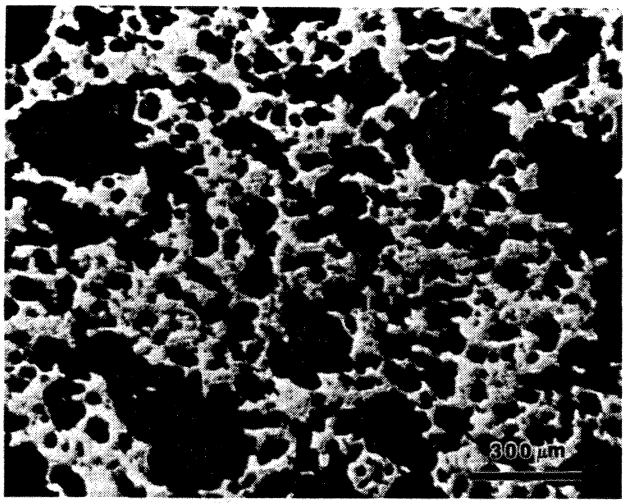

Fig. 1. Microstructure of reaction-synthesized TiC.

The powders were mixed according to the following reactions:

$$Ti + 0.9C \rightarrow TiC_{0.9} \quad (1)$$

$$Ti + 0.9C + (5\ wt\%)Ni \rightarrow TiC_{0.9} + (5\ wt\%)Ni \quad (2)$$

$$Ti + 0.9C + (25\ wt\%)Ni \rightarrow TiC_{0.9} + (25\ wt\%)Ni \quad (3)$$

In each of the reactions, excess titanium was used for two reasons. First, because of the often violent expulsion of impurities (i.e., outgassing) associated with this process, some titanium is inherently expelled from the compact.[30] Second, yield strength measurements at elevated temperature show that nonstoichiometric TiC has a lower yield strength than stoichiometric TiC.[31] The majority of the results (microstructural, mechanical, fracture characterization) in this paper are for reaction (1), while preliminary results (microstructure) concerning reactions (2) and (3) are briefly given. It should also be mentioned that there is experimental evidence that the products of reactions (2) and (3) may not be as indicated. Rogachev *et al.*[32] in their study on the interaction of Ti, C, and Ni during reaction found that the binder consisted of Ti–Ni compounds depending upon the initial reactant composition. Wong *et al.*[33] examined reaction (3) using a time-resolved X-ray diffraction technique. They also determined that a Ti–Ni compound formed during the reaction. Thus, based upon these experiments, the final product consists of a Ti–Ni compound (binder) and TiC grains closer to stoichiometry than indicated.

The powders were dry mixed in a ceramic grinding jar under an argon atmosphere. During the dry mixing process, a ceramic grinding medium was used. The grinding medium consisted of small cylindrical pellets composed of burundum (alumina/silica). Initial experiments were conducted without the use of the grinding medium. However, sectioning of the specimens after forging revealed large carbon agglomerates. In addition, an extensive network of cracks was observed to emanate from these agglomerations. Use of the grinding medium eliminated the presence of the carbon agglomerates and the related crack networks.

After mixing for approximately 4 h, the powders were compacted in a stainless steel die using an axial stress of about 55 MPa. This corresponded to a green density of approximately 60% of the theoretical value. The diameter of the cylindrical green compacts was approximately 9.5 cm. The mass of the Ti + C compacts was varied between 400 and 600 g. The mass of the green compacts with the Ni additions was approximately 400 g. It was determined experimentally that 60% of the theoretical value for the green density permitted the handling of the green compacts, as well as ease of ignition. Higher green densities resulted in green compacts that proved more difficult to ignite and, in some instances, difficult to sustain the reaction. This observation can be explained in terms of the green compact bulk (or local) thermal conductivity. Essentially, the bulk thermal conductivity increases with increasing green density due to the increase in the number of contact points between particles, as well as to the enlargement of contact areas between particles. The higher the thermal conductivity, the faster the energy released in the reaction wave is conducted into the unreacted material ahead of it (called the heat-affected zone). In order for the reaction wave to propagate continuously, the unreacted material in the heat-affected zone must be raised to the so-called "ignition" temperature (the temperature at which the conversion of the reactants to the final product(s) is greatly accelerated). However, if the thermal conductivity of the unreacted material is sufficiently high, this temperature will not be attained because the energy released by the reaction will be distributed over a larger volume of unreacted material. Thus, the heat-affected zone is effectively enlarged while the maximum temperature of this zone is effectively reduced. This leads to the extinction of the reaction.

The forging operation was performed using a modified Dynapak machine, Model 400. This machine was originally developed by General Dynamics/Electro Dynamic, Avenel, NJ, during the late 1960s for metal alloy forming applications. Figure 2 shows a schematic representation of the machine in the "safe" and "impact" positions. The main component of the machine is a gas-propelled hammer, where the potential energy stored in compressed nitrogen gas is transformed into the kinetic energy of the hammer. Hammer velocities typically range between 5 and 15 m/s at impact, depending upon the nitrogen gas pressure and stroke length. During normal operations, this machine can forge small billets (or blanks) into engineering parts 20 times per minute at the maximum rated safe energy output of 17 kJ (at a nitrogen pressure of 13.8 MPa and a stroke length of 23 cm). For our research purposes, this machine was slightly modified. The hydraulic system was originally operated off of three hydraulic pumps. These were replaced with a 5-hp hydraulic pump and 5 gal oil/nitrogen accumulator. Other modifications include the installation of an exhaust cleaner and enclosing the work area of the machine. The exhaust cleaner is used for removing the outgassing impurities from the laboratory air. Enclosing the work area of the machine decreases the chance for hot debris being scattered about in the laboratory. The energy output of the machine was increased to approximately 25 kJ by operating at a maximum nitrogen gas pressure of 20.7 MPa.

During the forging operation, the compact is contained in a specimen containment fixture which is shown schematically in Fig. 3. The purpose of the specimen containment fixture is to fully contain the reaction-synthesized product during both the reaction and the forging process. It also serves the additional purpose of protecting the lower die cavity walls from the extreme heat evolved during the reaction and excessive wear due to forging. The main components of the specimen containment fixture are a tapered steel ring and refractory insulation (Zircar Products, Inc., Florida, NY). The steel ring is tapered to allow easy removal from the cavity after forging. The refractory insulation is glued to the inner radius of the steel ring. Initial designs used zirconia felt (Zircar Products) instead of the refractory insulation. However, the zirconia felt failed to provide adequate thermal insulation. The hard refractory insulation serves two purposes. The first purpose is to prevent the compacts from cooling too rapidly during forging by heat conduction from the compact to the lower die. The lower die is heated to a temperature between 100° and 200°C; however, this is done only to increase its toughness rather than decreasing compact heat losses. The second purpose is to provide lateral confinement of the compact during forging. This is especially important, since with lateral con-

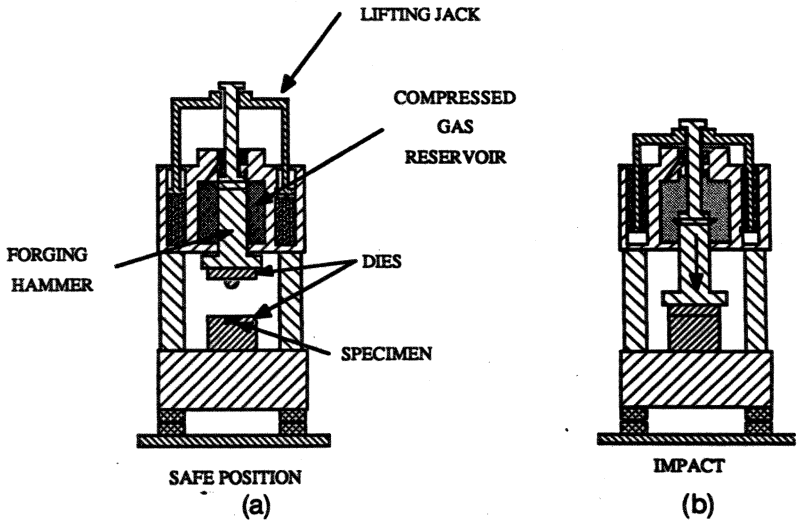

Fig. 2. Dynapak high-velocity forging machine: (a) loading position; (b) impact position.

finement the pressure within the compact can attain a higher value (thus aiding densification) than that possible when no lateral confinement is used. A layer of grafoil (Union Carbide Corp., Electronics Division, Cleveland, OH) was used between the compact and the refractory insulation. This grafoil layer serves as a lubricant and diffusion barrier between the compact and refractory insulation during forging.

The technique used to ignite the green compacts was originally developed by Niiler and co-workers.[23] It consists of placing uncompacted reactant powder on the top surface of the green compact. This uncompacted powder is then ignited by using an "electric" match (i.e., rocket ignitor; Estes industries, Penrose, CO). The energy released from the uncompacted powder is then sufficient to ignite the top surface of the green compact. Once the reaction is initiated, it quickly propagates (velocity approximately 2 cm/s) in the form of a reaction wave through the remaining unreacted material. The amount of uncompacted powder used in an experiment was typically one-tenth the mass of the green compact.

After the green compact has been fully converted into the final product, the resulting porous microstructure (as shown in Fig. 1) is collapsed by the forging process. Earlier densification studies recognized a time "window" in which successful densification could be accomplished.[9,23] This window is typically measured in seconds, and is highly system dependent. For our system, densification typically occurred between 5 and 10 s after ignition. After densification, the compact is placed in a 1100°C furnace with argon atmosphere for controlled cooling. The compact is allowed to cool over a 12-h period. Finally, the compact is removed from its containment fixture and machined.

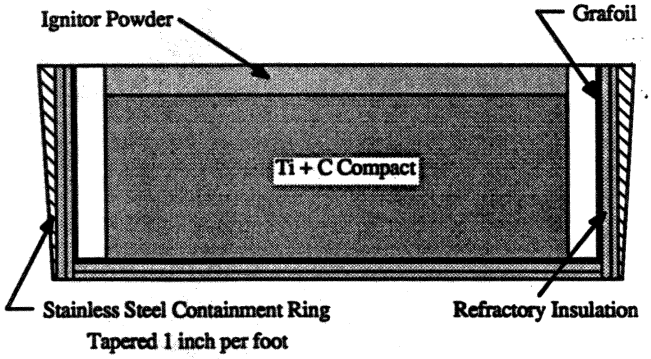

Fig. 3. Schematic diagram of the specimen containment assembly with green compact.

Bulk density measurements were made using the water immersion technique and a theoretical density of 4.88 g/cm^3 for the reaction-synthesized TiC (theoretical density for the product $TiC_{0.9}$). The machined compacts were sectioned for metallographic examination and mechanical measurements. Specimens for optical examination were polished using colloidal silica (0.05 μm) and etched with a solution consisting of 2 parts nitric acid, 1 part hydrofluoric acid, and 1 part acetic acid for approximately 30 s. Grain size measurements were made by the line-intercept method. Here, the as-measured linear intercepts were multiplied by a numerical factor of 1.5 to convert to a "true" grain size.[34] Vickers microhardness measurements were conducted using a load of 300 g. A minimum of 30 measurements were made on each compact that was examined. Quasi-static and dynamic compressive strength measurements were conducted at IFAM on cubical-shaped specimens with 6-mm sides. The quasi-static tests were performed at a strain rate of 10^{-4} s^{-1}. Dynamic compressive mechanical tests were conducted in a drop hammer machine. A strain gage attached to the specimen provided the fracture load; the strain rate was approximately 10^2 s^{-1}. In both the static and dynamic tests, careful attention was made to ensure that the specimen-loading axis alignment and the flatness of the load-bearing specimen interfaces were sufficient to provide a nearly homogeneous compressive stress distribution within the specimens. Tool steel plates hardened to 62 HRC with $MoSi_2$ lubrication in a fixture developed at IFAM were used for both quasi-static and high-strain-rate mechanical tests.[35] The reaction-synthesized TiC with Ni addition specimens were metallographically examined. Final polish was accomplished using 0.25-μm-diamond paste.

A commercially produced piece of TiC (Cercom Inc., Vista, CA) produced by hot-pressing was obtained for the purpose of comparison with the reaction-synthesized/forged TiC. Metallographic examination and Vickers microhardness measurements were also performed.

III. Results and Discussion

(1) Compact Integrity

The measured bulk and center densities for the 10.16-cm compacts after forging are shown in Fig. 4 as a function of specific energy (i.e., machine energy divided by the mass of the compact). The specific energy listed represents an upper bound for two reasons. The first reason is that in operating the machine at nitrogen pressures greater than those normally used, the energy in the machine was estimated from the energy vs pressure data (which is linear) for the machine by assuming a continued linear variation at the higher pressures.

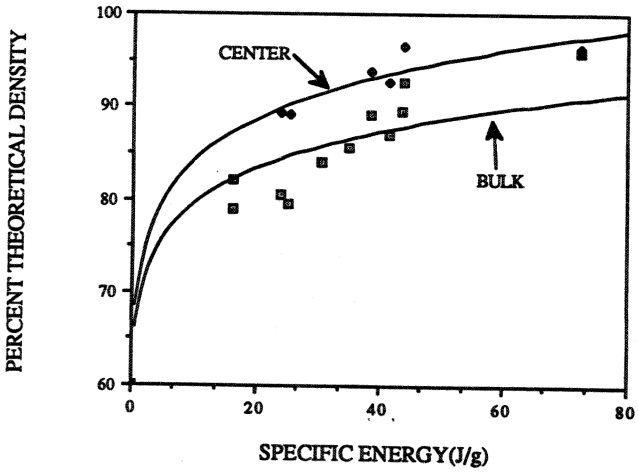

Fig. 4. Density as a function of specific energy.

The second reason is that in any forging process, the machine energy is not fully converted into deformation energy. Some energy is inherently lost because of elastic deflections within the machine itself. As can be seen in Fig. 4, the bulk densities are consistently lower than the center densities. Based upon the fact that the flow strength of the material is temperature dependent and that there are heat losses taking place before the forging operation, one could reason that the porosity near the surface of the compact would be higher than in the bulk. This is indeed confirmed by both visual and light microscope examination. The porous layer near the top and bottom surfaces is typically 2 mm thick, while near the lateral surfaces, it is normally several millimeters thick. The maximum bulk and center densities approached 97% (4.73 g/cm^3) of the theoretical. Further increases in specific energy did not result in higher densities. Examination of these compacts revealed partial extrusion between the hammer and the inner wall of the specimen containment fixture. The compressive strength of the refractory insulation is approximately 100 MPa. As the specific energy is increased, the pressure within the compacts correspondingly increases. This pressure is transmitted to the refractory insulation by the specimen. Eventually, the pressure on the refractory insulation is sufficient to cause its failure, thereby increasing the annular gap between the refractory insulation and the hammer. This increase in the gap permits a path of least resistance for the compact to follow.

Shown in Fig. 5(a) is an early attempt to densify a TiC compact. The most severe problem encountered in this work has been cracks that extend through the thickness of the compacts. These cracks appear to be the result of thermal shock and possibly overforging (exceeding the ductility of the material in tension). The evidence for overforging is seen in cracks which start at the lateral surface and propagate toward the center of the compact (i.e., tearing). In addition, an engineering radial strain of approximately 7% is experienced by the compact during the forging process (in going from a diameter

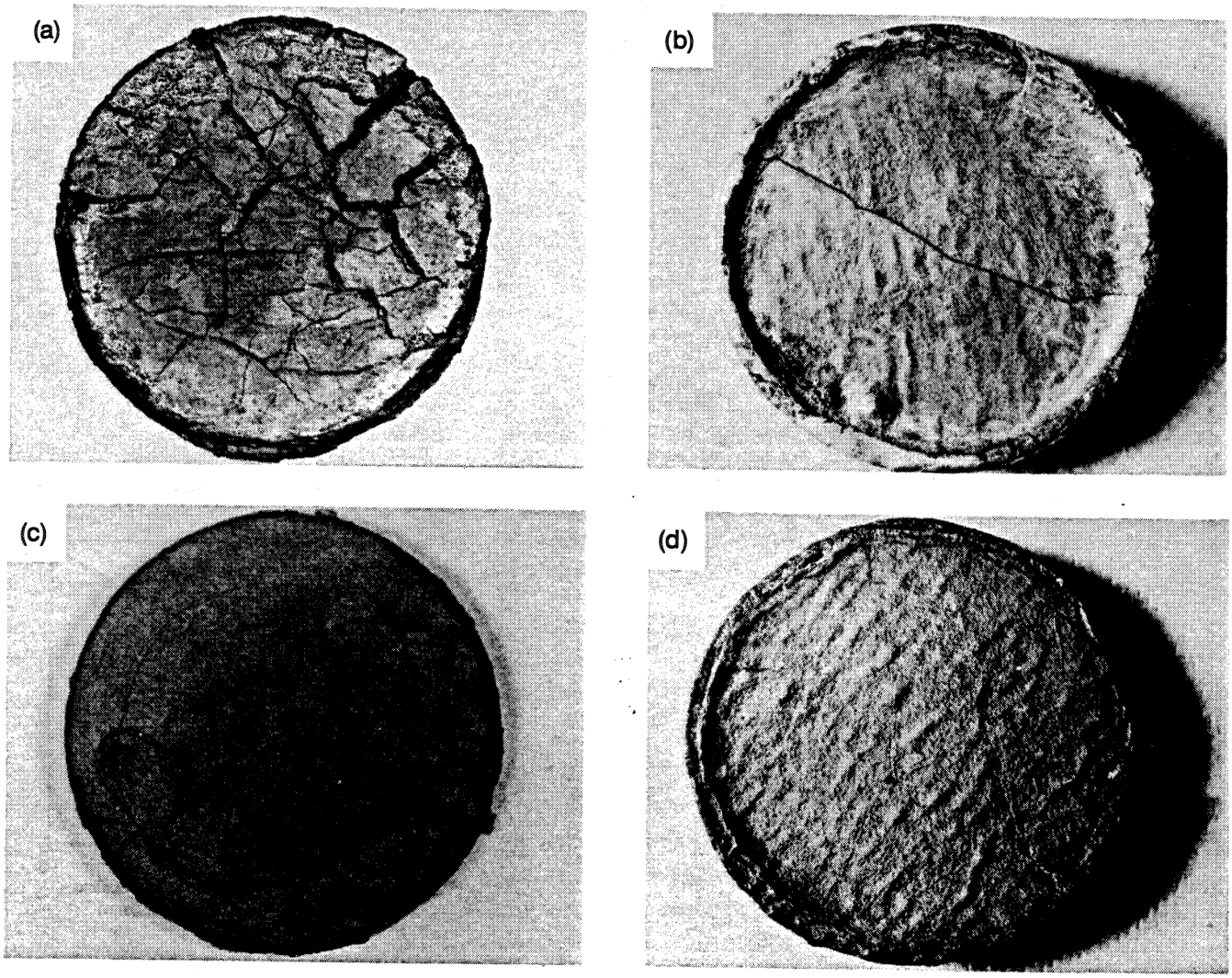

Fig. 5. (a) Initial compaction results. (b) Later compaction results. (c) Circumferential cracks. (d) "Healed" hot-tearing cracks.

of 9.5 to 10.16 cm). This strain, if not accommodated, can lead to residual stresses and an increased likelihood of crack formation. Solution to this problem would require providing enough lateral confinement so as not to allow circumferential strains from exceeding the critical rupture strain in tension. A solution to the thermal shock problem requires the promotion of a uniform temperature distribution within the compact both during and after the forging operation (postforging cool-down period). This can be done by combining the use of insulation with heating of the compact surroundings. Heating of the compact surroundings should ideally be included during forging (i.e., hot-forging) and during cooling. We have chosen the latter because of laboratory restrictions. Figure 5(b) shows the results of the combined use of insulation and furnace cooling. The severity of the thermal shock problem has been reduced.

Three types of macrocracks are observed to be dominant. All three are a major consequence of nonuniform cooling. In some instances, overforging may also be an important factor in their development. The first type is the radial crack. This is shown in Fig. 5(b). This type of crack is the most commonly observed. Because of the axisymmetry of the reaction synthesis/forging process, the largest variations in temperature within the compact will occur in the radial direction (the outer surface being cooler than the interior of the compact). Since strength is temperature dependent, the outer surface being cooler (hence, stronger) constrains the contraction of the interior as it begins to cool. Because the interior is unable to contract, both radial and tangential stresses develop. The tangential stresses are tensile and, therefore, provide the necessary driving stress for the development of the radial cracks. The second type is the circumferential crack. This is shown in Fig. 5(c). Two types of circumferential cracks have been observed. One type appears to separate regions of high porosity and nearly dense material. They are typically found within several millimeters from the lateral edge of the compacts. The other, as shown in Fig. 5(c), forms farther away from the lateral edge of the compacts. It has been observed that the formation of the circumferential cracks suppresses the formation of the radial cracks. The third type of crack is unlike the other two types in that it does not extend through the thickness of the compact. They are found on the top and bottom surfaces of the compacts, and extend only a couple of millimeters into the compact. Because of heat losses, these surfaces become hardened. During forging, these surfaces become fragmented. This phenomenon is usually referred to as "hot-tearing."[36] Because these hardened surfaces fragment, the more ductile bulk material is able to flow into the tears, thereby healing them. Figure 5(d) shows "healed" hot-tearing cracks.

By tailoring the insulation around the compact, it is possible to alter the configuration of the cracks and eventually eliminate them. The circumferential cracks were found to be caused primarily by differences in heat transfer between the radial and axial directions. Figure 6(a) shows a schematic of the densified TiC compact enclosed within the specimen containment assembly. Also depicted are the top, bottom, and lateral insulations, with heat transfer directions indicated by the respective arrows in regions I, II, and III. When the heat losses I and III (axial) are increased (by decreasing the thickness of the top and bottom insulation) with respect to II (radial), the position of the circumferential cracks changes, moving closer to the external lateral surface. This is clearly shown in Fig. 6(b). Conversely, by decreasing the thickness of the insulation along the lateral surface of the compacts with respect to the top and bottom insulation, the circumferential cracks form closer to the center of the compacts. The lateral insulation thickness to radial insulation thickness ratio was eventually reduced to one-half, leading to the elimination of the circumferential cracks.

(2) *Microstructural Characterization*

Optical microscopy revealed that the microstructure of the reaction-synthesized/forged TiC consists of equiaxed grains approximately 44 μm in size. Figure 7(a) is an optical micrograph showing the microstructure; the dark "spots" are residual porosity. The equiaxed grain structure clearly shows that the grains formed after the deformation process; if they were formed prior to densification, they would be correspondingly distorted (i.e., elongated). Figure 7(b) is an optical micrograph which shows the microstructure of the commercially produced TiC. The grain size of the commercially produced material was determined to be approximately 30 μm. As can be clearly seen in this figure, a uniform distribution of intragranular voids appears throughout the microstructure. Figure 8(a) is a scanning electron micrograph of the reaction-synthesized/forged TiC showing the porosity at higher magnification. Two types of voids are commonly observed: large, irregularly shaped voids and small, faceted voids. A large, irregularly shaped void is shown in Fig. 8(b). The large voids appear to be remnants of the porous microstructure associated with the reaction synthesis process because of their irregular shape. The majority of these voids are found to be located at grain boundaries. The smaller voids are thought to be due to the presence of dissolved impurity gases; however, it is also a possibility that they are formed because of the differing reactant and product densities. These voids are mainly found in the interior of grains. Figure 8(c) is a scanning electron micrograph showing the porous microstructure

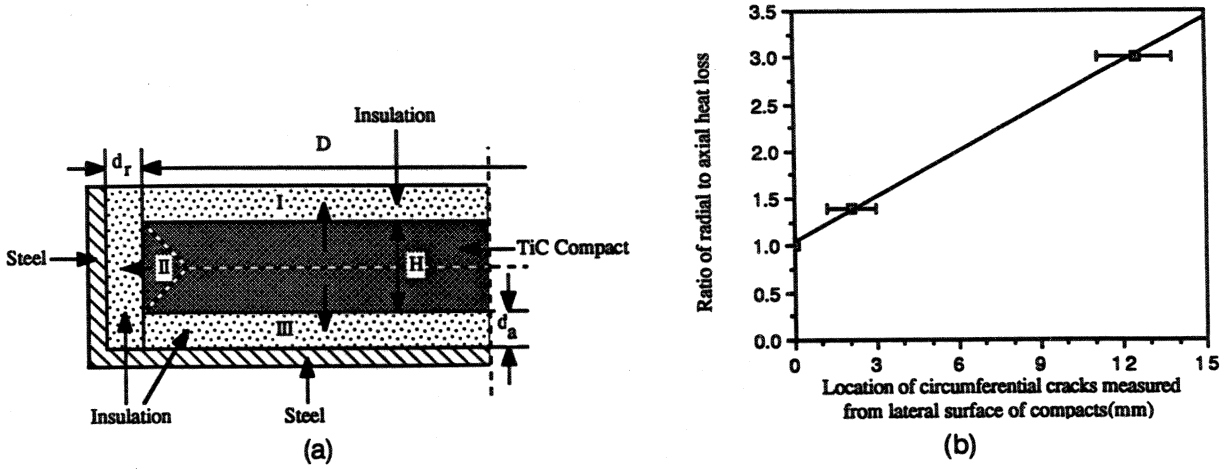

Fig. 6. (a) Schematic representation of heat loss from compacted specimen in directions I, II, III. (b) Effect of the radial to axial heat loss on the location of circumferential cracks in compact.

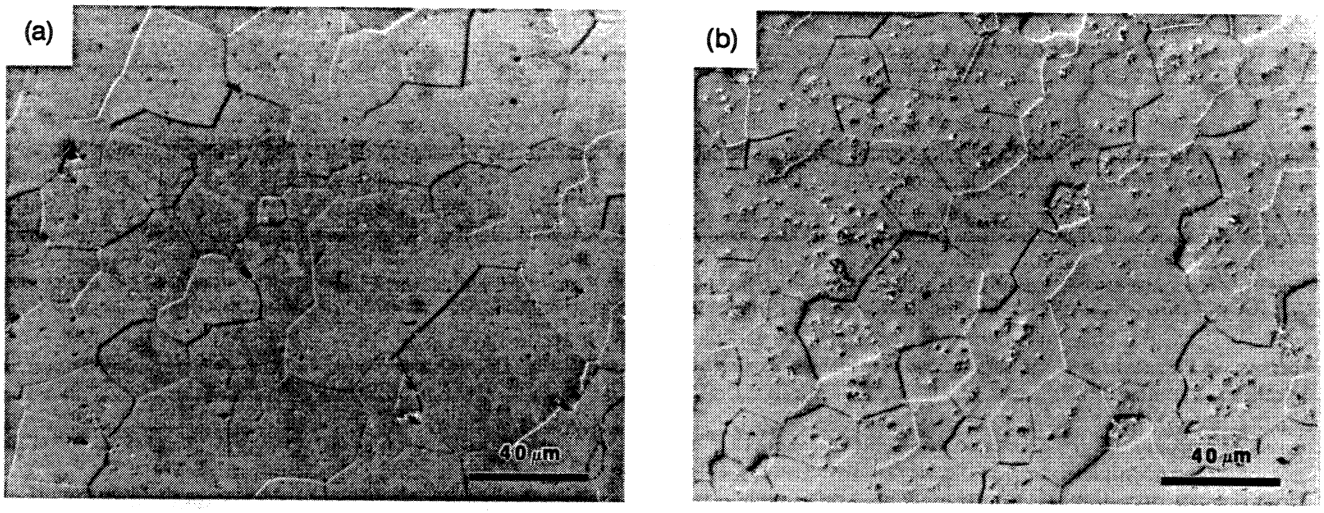

Fig. 7. Optical micrographs of (a) reaction-synthesized/forged TiC microstructure; (b) commercially produced TiC microstructure.

of the commercially produced TiC more clearly. In addition to intragranular voids, grain boundary separation and voids at grain boundary triple points are seen (incomplete sintering). While density measurements of this material provide values in excess of 99% of the theoretical (4.92 g/cm^3), the apparent porosity would seem to indicate that it is actually lower. Electron dispersive spectroscopy of this material has revealed the presence of minute quantities of both Fe and Co (the Co peak was much larger than the Fe peak). Co is often used as a sintering aid for TiC.[37] The quantities of both elements that were detected appear to be too small to have any real effect on the overall density of the material. However, if the void

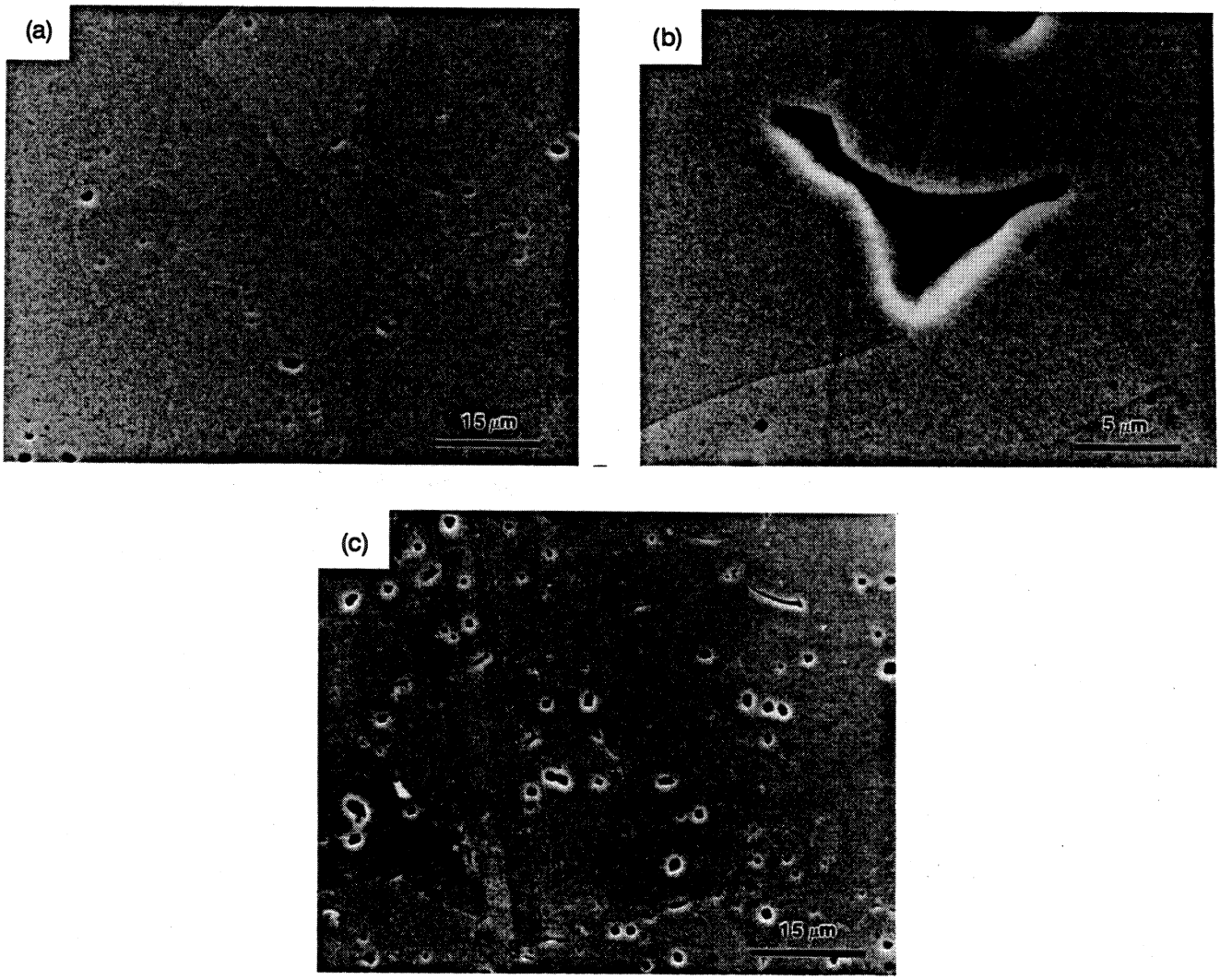

Fig. 8. Scanning electron micrograph showing the residual porosity in (a) reaction-synthesized/dynamically compacted TiC; (b) irregularly shaped void in the reaction-synthesized/forged TiC; (c) commercially produced TiC.

volume percent is estimated to be approximately 2%, than the Co volume percent necessary to achieve a measured density in excess of 99% of the theoretical density is only 2.5%. This corresponds to a Co mass percent of approximately 4.5%. Thus, not much Co would be needed to obtain a density measurement close to the theoretical. The substructures of both the reaction-synthesized/forged and commercially produced TiC are examined in more detail by Vecchio *et al.*[38]

The effect of additions of 5 and 25 wt% Ni on the reaction-synthesized/forged TiC microstructure is shown in Figs. 9(a) and (b), respectively. Porosity is clearly seen in Fig. 9(a). The reason for this porosity is not clearly understood since it is expected that the Ni is in a beneficial transitory liquid phase during the reaction synthesis process. This liquid phase should facilitate the collapse of the porous microstructure during the forging process since it cannot support shear. A possible explanation for this porosity is that the reaction had not undergone completion when the compact was forged. Aside from the porosity, the TiC grains appear to be equiaxed with a thin layer of Ni (arrow A) located between the grains. The Ni layer does not appear to be continuous. Increasing the Ni addition to 25 wt% results in smaller spheroidal-shaped TiC grains embedded in a Ni (or Ti–Ni compound) matrix. The composite appears to be fully dense. Because of the incomplete wetting of the TiC grains by the Ni melt during synthesis, coarsening of the TiC grains can be seen. The addition of Mo leads to better wetting and the elimination of grain coarsening.[39] It is of interest to note that while the reaction wave for the 5 wt% Ni addition was observed to propagate in a stable manner, the reaction wave for the 25 wt% Ni addition propagated in an unstable manner. During the reaction, two bright "spots" on the lateral surface of the compact appeared to propagate in a helical manner down the compact. One spot moved in a clockwise direction, while the other moved in a counterclockwise direction. This propagation mode has been experimentally observed in a number of systems.[40–44]

An upper bound estimate of the flow stress for reaction-synthesized TiC can be made by assuming that all of the mechanical energy is converted into plastic deformation energy. The Carroll and Holt model[45] (also referred to as the "hollow-sphere" model) predicts satisfactorily the energy required to consolidate a porous material. This model predicts that the energy per unit mass required to collapse a ductile porous body is given by

$$E = \frac{2}{3\rho}\sigma_y[\alpha_0 \ln \alpha_0 - (\alpha_0 - 1)\ln(\alpha_0 - 1) - \alpha \ln \alpha + (\alpha - 1)\ln(\alpha - 1)] \quad (4)$$

where E is the deformation energy per unit mass, ρ is density of the matrix, σ_y is the flow stress of the matrix, α_0 is the initial ratio of the specific volume of the compact to the specific volume of the matrix, and α is the final ratio of the specific volume of the compact to the specific volume of the matrix. For a density of 96% of the theoretical, from Fig. 4, E is approximately 74×10^3 J/kg. For α_0 equal to 2 (50% dense) and α equal to 1.04 (96% dense), Eq. (4) yields an estimate of the flow stress for the reaction-synthesized TiC equal to approximately 370 MPa. This is quite high since Katz *et al.*[29] measured the flow stress at 1700°C to be close to 100 MPa, while Toth[27] reports that the flow stress is approximately 50 MPa at 1800°C. Given that the maximum temperature for the reaction-synthesized TiC is in excess of 2000°C, the high flow stress estimate using Eq. (4) could be due to a strain-rate sensitivity of the material. The initial strain rate imparted to the material during forging is approximately 10^3 s^{-1}, while the measured flow stresses are for much lower strain rates (10^{-4} to 10^{-3} s^{-1}). However, as mentioned previously, not all of the energy stored in the machine is converted into deformation energy. The actual usable energy depends upon the characteristics of the forging operation. A forging operation is normally associated with a blow efficiency (actual energy delivered to the workpiece/energy stored in the machine). Blow efficiencies typically range from 0.2 to 0.4 for "hard" blows and from 0.8 to 0.9 for "soft" blows.[46] Hard blows are characterized by high loads and small displacements, while soft blows are characterized by low loads and large displacements. Based upon a displacement of 1.5 cm and an estimated maximum load of 1.335 MN (150 tons), we believe that we are in the "hard" blow forging regime. This is substantiated by the study of Dorofeev and Prutsakov[47] on the energy absorption of metal powders during high-velocity forging. They measured blow efficiencies between 0.1 and 0.4, depending upon the initial porosity and velocity of the hammer (decreasing blow efficiencies for increasing initial porosity and increasing hammer velocity). Based upon these experimental data, if we assume a blow efficiency of 0.4, a flow stress of 148 MPa is obtained.

(3) Mechanical Measurements

The variation of the mean Vickers microhardness number with density is shown in Fig. 10. Both minimum and maximum recorded values, as well as the standard deviation of the measurements, are also shown. The standard deviation, as expected, decreases with increasing density because of the decreasing probability of void-measurement interaction. The mean Vickers microhardness number for the 96%+ dense compact was 2257 HVN with a standard deviation of 193.

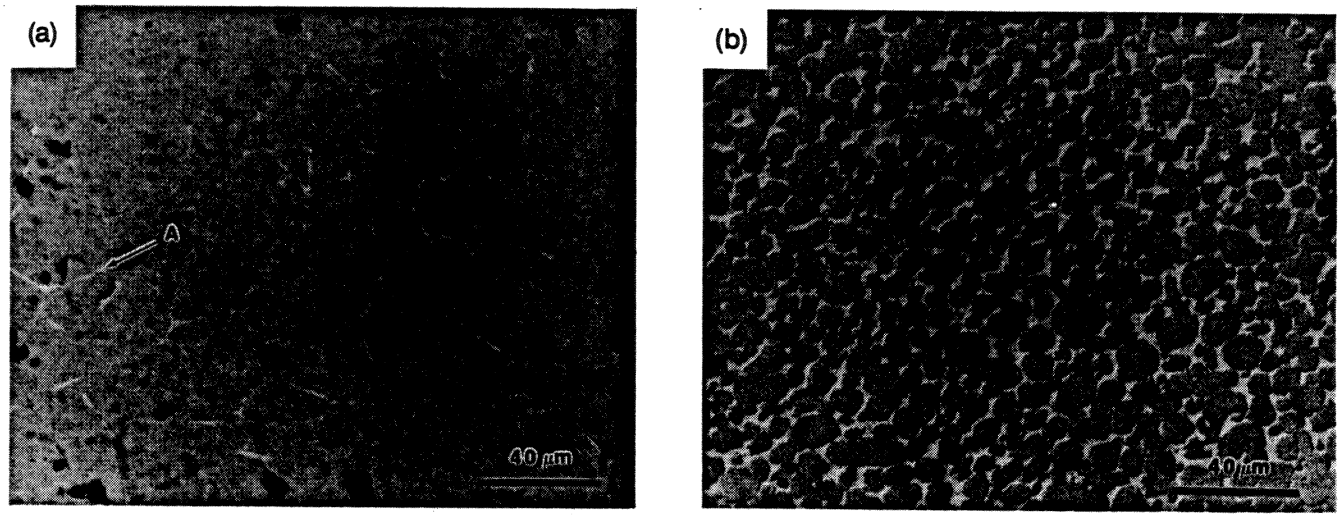

Fig. 9. Optical micrographs showing the effect of Ni additions on the reaction-synthesized/forged TiC microstructure for (a) 5 and (b) 25 wt%.

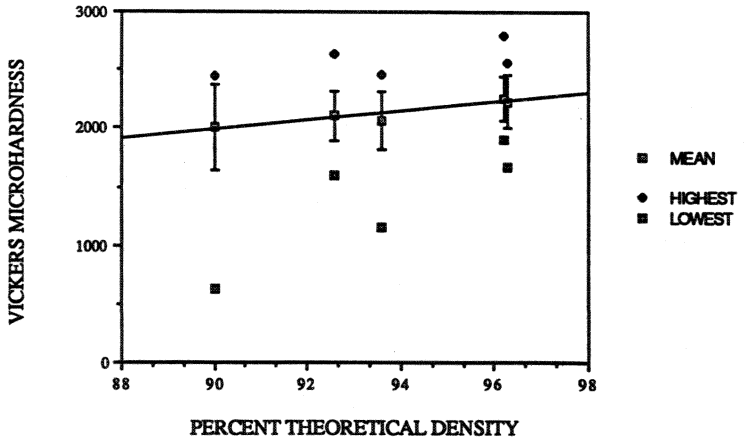

Fig. 10. Vickers microhardness as a function of density.

For comparison, the mean Vickers microhardness number for the commercially produced material was 2235 HVN with a standard deviation of 248. Several Vickers microhardness profiles across the cross section (top to bottom) of the 96%+ dense compact were made in order to determine whether or not the microstructure was homogeneous. Because of the possible large temperature gradients within the compact, the microstructure was not expected to be homogeneous. Indeed, light-microscopy examination showed smaller grains near the surface and larger grains in the central region. The average value of the profiles is shown in Fig. 11. There is a noticeable oscillation, as well as a slight increase going from the top surface to the bottom surface in the profile. The oscillation in the profile is not due to the averaging of the profiles; each profile consistently exhibited this oscillation (averaging does make the oscillations more noticeable). This oscillation was later confirmed by etching; bands parallel with the top surface were observed. These bands constituted areas which were etched more severely than the rest of the cross section. This is shown in Fig. 12. The true nature of these bands is not known since they were not observed in every compact, and could be an artifact introduced during machining. However, it has been observed experimentally[44] and shown by theoretical modeling[48] that the reaction wave can propagate in a number of unstable modes. One such mode is characterized by oscillations in the temperature profile. It is therefore possible that the bands revealed by chemical etch are the result of this unstable reaction wave propagation mode. The slight increase in the microhardness of the material in going from top to bottom may be explained by the fact that the bottom surface of the compact cools down more rapidly than the top surface because of heat losses through the bottom insulation sheet and because the reaction wave propagates from top to bottom. This might result in a slight decrease in grain size or an increasing dislocation density between the top surface and the bottom surface.

The results of the static and dynamic compressive strength measurements as a function of density are shown in Fig. 13. The maximum quasi-static compressive strength was measured to be 1.79 GPa at a strain rate of 10^{-4} s^{-1}. A maximum high-strain-rate compressive strength of 2.29 GPa was obtained at a strain rate of 10^{2} s^{-1}. In both cases, the compressive strength increases with increasing density, as expected. There is a clear strain rate dependency on the compressive strength.

(4) Fracture Characterization

Figure 14(a) shows a scanning electron micrograph of a fracture surface obtained during a high-strain-rate loading test for the reaction-synthesized/forged TiC. The cracks propagated primarily in the transgranular mode with some evidence of the intergranular mode. The crack propagation direction was found to be parallel to the loading axis (i.e., axial splitting). Figure 14(b) shows the fracture surface at higher magnification. Clearly seen is an irregularly shaped void

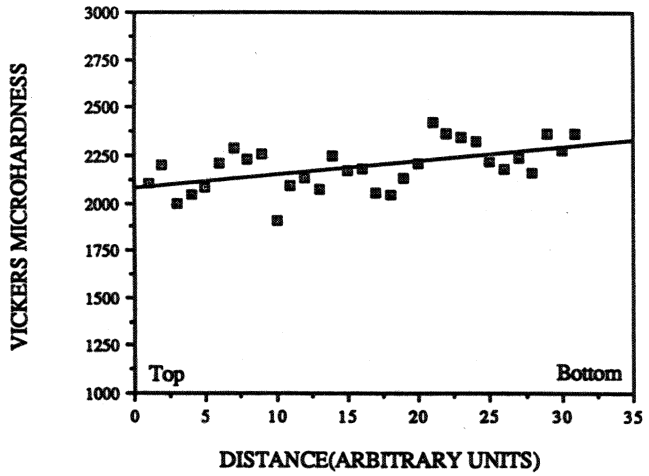

Fig. 11. Vickers microhardness cross-sectional profile.

Fig. 12. Banded regions on the reaction-synthesized/forged TiC that have undergone severe reaction to the chemical etching process.

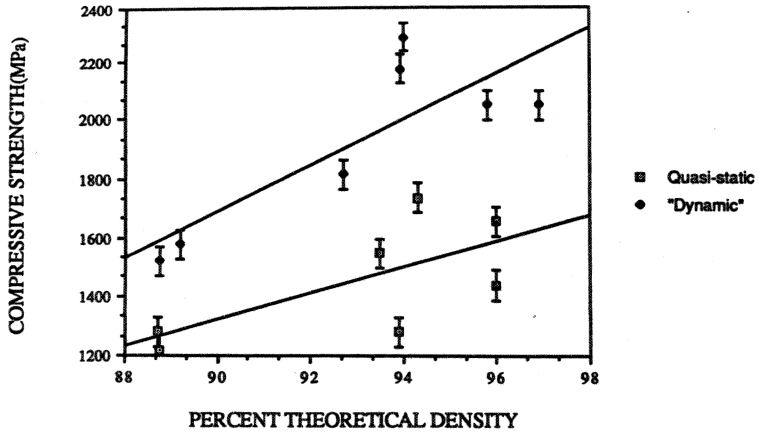

Fig. 13. Compressive strength as a function of density and strain rate. Quasi-static and high-strain-rate loading at 10^{-4} and 10^{2} s^{-1}, respectively.

which was not collapsed during the forging process. The fracture morphology for the commercially produced TiC obtained under impact loading conditions is shown in Fig. 15. Intragranular porosity is clearly seen.

Fracture produced by thermal gradients (thermal gradients caused by heat loss from the compact during processing), on the other hand, exhibits a markedly different morphology. The fracture mode was primarily intergranular, as shown in Fig. 16(a). Profuse oxide growth on grain surfaces and grain boundaries is clearly seen. Oxidation probably occurred during cooling, after the opening of the cracks exposed these surfaces to the air. Figure 16(b) shows the oxide growth at higher magnification. According to Voitovich and Golovko,[49] the oxide growth is connected to the formation of titanium oxycarbides by the solution of oxygen ions (low oxygen concentration) into the titanium carbide lattice via grain boundaries and dislocation lines. The formation of titanium oxycarbides is said to be followed by the precipitation of titanium at grain surfaces and grain boundaries. These precipitates are subsequently oxidized, normally forming lower oxides of titanium. Figure 16(c) shows the oxide growth in the grain boundaries (arrow A). The oxide growth at the grain boundaries has appeared to coalesce together, forming a continuous grain boundary oxide layer. Figure 16(d) shows cracks located at grain junctions. The formation of these cracks is possibly not unlike the spallation of an aluminum oxide film on aluminum. Here, oxidation induces tensile stresses at grain junctions. Grain junctions, being inherently weaker than the bulk material, fail when these tensile stresses reach a critical value.

IV. Summary

A new technique for simultaneous densification and forming of ceramic materials is being studied. The ceramic materials are produced by reaction synthesis, while the densification and forming is accomplished by a high-velocity forging machine. This technique was used to produce dense titanium carbide disks 10.16 cm in diameter. The highest density achieved was greater than 96% of the theoretical density. Loss of lateral confinement during forging has prevented the achievement of higher densities.

The microstructure consists of equiaxed grains approximately 44 μm in size. Porosity consisted of large, irregularly shaped voids (residual initial porosity) located at grain boundaries and small, faceted voids located predominately within the grains.

Vickers microhardness measurements indicate values comparable with a commercially produced material. Quasi-static (10^{-4} s^{-1}) and high-strain-rate (10^{2} s^{-1}) compressive strength measurements yielded values greater than 1.7 and 2.2 GPa, respectively.

The major problem encountered in this work has been thermal shock, with overforging a possible contributing factor. Use of insulation in the specimen containment assembly and inert-atmosphere furnace cooling have decreased the severity

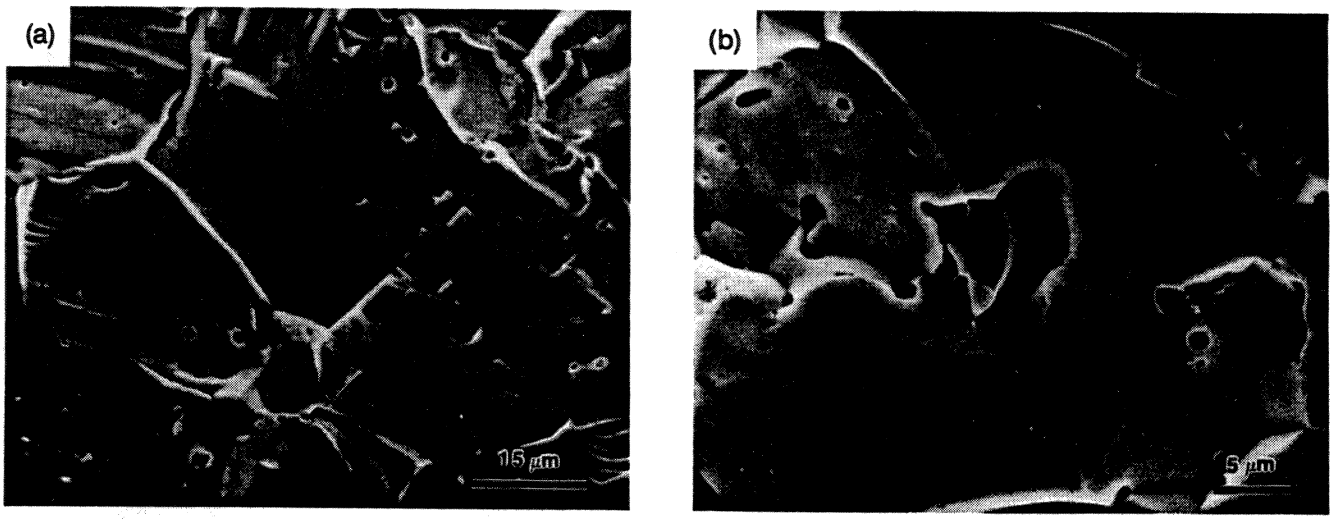

Fig. 14. (a) Scanning electron micrograph of TiC fracture surface obtained after high-strain-rate loading. (b) Transgranular fracture surface at higher magnification showing an irregularly shaped void.

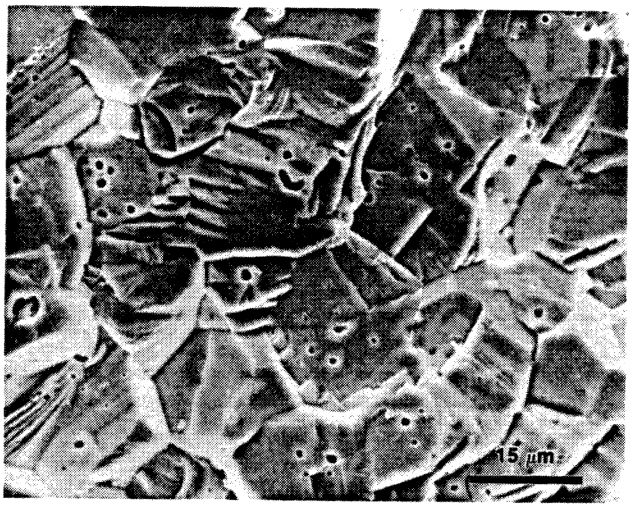

Fig. 15. Fracture morphology of commercially produced TiC obtained under impact loading conditions.

of this problem. However, this problem remains to be solved (at least for titanium carbide). Recent work has indicated that the inert-atmosphere furnace cooling is not very effective, at least, for this experimental setup. This indicates a different solution strategy than the one pursued in this paper, such as by combining the reaction synthesis/forging process with the CERACON[50] technique.

Preliminary results with the addition of 5 and 25 wt% Ni were also presented. The TiC grains are primarily equiaxed in the 5 wt% composite, while in the 25 wt% composite they are spheroidally shaped. Porosity was observed in the 5 wt% composite, while the 25 wt% composite appears to be fully dense. Because of incomplete wetting of the TiC grains by the Ni melt, grain coarsening is observed.

Acknowledgments: The support and encouragement of Dr. A. Crowson, Program Manager, is gratefully acknowledged. The authors would like to thank Mr. Klaus Blueggel for his expert knowledge in modifying and operating the Dynapak machine, Mr. Darren Hoke for his advice throughout this investigation, and Mr. Li-Hsing Yu for his gracious assistance in much of this study. We would also like to thank Dr. Andrus Niiler (who spent a month working with us on this program), as well as interactions with his co-workers Dr. Thomas Kottke, Mr. Lazlo Kecskes, and Mr. Bart Pierce. The use of the facilities of the Center of Excellence for Advanced Materials is greatly appreciated. We thank Mr. Richard Policka, President of Cercom Inc., for his assistance in supplying the hot-pressed TiC.

References

[1]N. P. Novikov, I. P. Borovinskaya, and A. G. Merzhanov, "Thermodynamic Analysis of Self-Propagating High-Temperature Synthesis Reactions"; pp. 174–88 in *Combustion Processes in Chemical Technology and Metallurgy* (in Russ.). Edited by A. G. Merzhanov. Chernogolovka, Russia, 1975.

[2]Z. A. Munir, "Synthesis of High Temperature Materials by Self-Propagating Combustion Methods," *Am. Ceram. Soc. Bull.*, **67** [2] 342–49 (1988).

[3]J. F. Crider, "Self-Propagating High Temperature Synthesis—A Soviet Method for Producing Ceramic Materials," *Ceram. Eng. Sci. Proc.*, **3**, 519–28

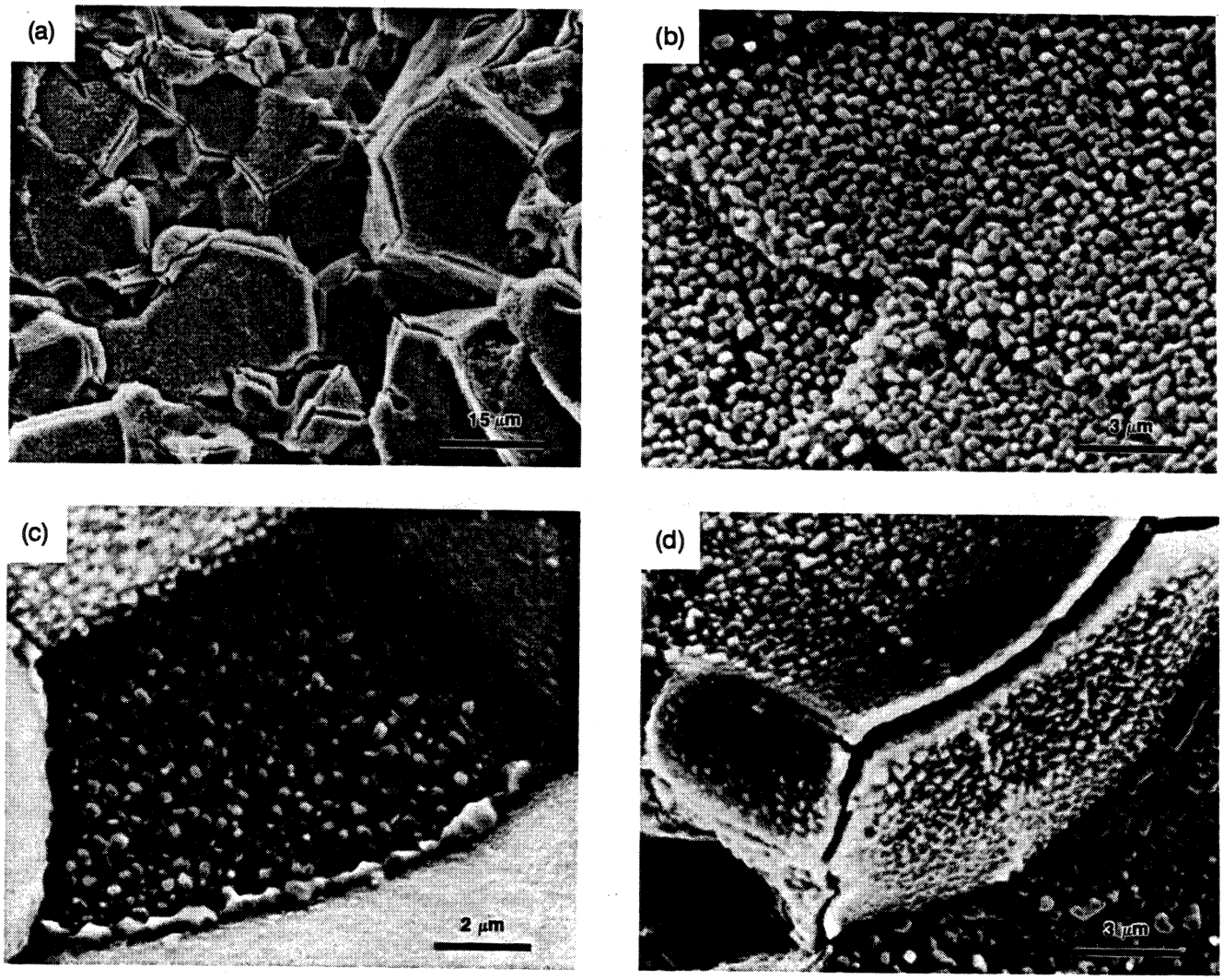

Fig. 16. Thermally induced fracture surface: (a) grain surface oxidation of either titanium and/or lower titanium oxides, (b) oxide growth, (c) continuous layer of oxide at a grain boundary (arrow A), (d) grain junction cracks or splitting (arrow A).

(1982).
[4]W. L. Frankhouser, K.W. Brandley, M. C. Kleszek, and S.T. Sullivan, *Gasless Combustion Synthesis of Refractory Compounds.* Noyes Publications, Park Ridge, NJ, 1985.
[5]Z. A. Munir and U. Anselmi-Tamburini, "Self-Propagating Exothermic Reactions: The Synthesis of High-Temperature Materials by Combustion," *Mater. Sci. Rep.*, **3**, 277–365 (1989).
[6]P. Hardt, "Review of Self-Propagating High-Temperature Synthesis Technology," Lockheed Missiles and Space Company Inc., LMSCD879371, Contract DAAG46-84-0355, Army Materials and Mechanics Research Center, Watertown, MA.
[7]J.W. McCauley, "An Historical and Technical Perspective on SHS," *Ceram. Eng. Sci. Proc.*, **11** [9–10] 1137–81 (1990).
[8]J. B. Holt, "The Use of Exothermic Reactions in the Synthesis and Densification of Ceramic Materials," *MRS Bull.*, **12**, 60–64 (1987).
[9]A. G. Merzhanov, "Self-Propagating High-Temperature Synthesis: Twenty Years of Search and Findings"; pp. 1–53 in *Combustion and Plasma Synthesis of High Temperature Materials.* Edited by Z. A. Munir and J. B. Holt. VCH Publishers, New York, 1990.
[10]R. M. German, *Liquid Phase Sintering.* Plenum, New York, 1985.
[11]KRI Kiser Research, Inc., Washington, DC, "Trip Report on Soviet SHS Technology," pp. 1–11, January 1989.
[12]Y. Miyamoto, M. Koizumi, and O. Yamada, "High-Pressure Self-Combustion Sintering for Ceramics," *J. Am. Ceram. Soc.*, **67** [11] C-224 (1984).
[13]O. Yamada, Y. Miyamoto, and M. Koizumi, "High-Pressure Self-Combustion Sintering of Titanium Carbide," *J. Am. Ceram. Soc.*, **70** [9] C-206–C-208 (1987).
[14]S. Adachi, T. Wada, T. Mihara, M. Koizumi, and O. Yamada, "Fabrication of Titanium Carbide Ceramics by High-Pressure Self-Combustion Sintering of Titanium Powder and Carbon Fiber," *J. Am. Ceram. Soc.*, **72** [5] 805–809 (1989)
[15]S. Adachi, T. Wada, T. Mihara, Y. Miyamoto, and M. Koizumi, "High-Pressure Self-Combustion Sintering of Alumina–Titanium Carbide Ceramic Composite," *J. Am. Ceram. Soc.*, **73** [5] 1451–52 (1990).
[16]D. M. Sims, A. Bose, and R. M. German, "Reactive Sintering of Nickel Aluminide," *Prog. Powder Metall.*, **43**, 575–96 (1987).
[17]J.W. McCauley, N. D. Corbin, T. Resetar, and P. Wong, "Simultaneous Preparation and Self-Sintering of Materials in the System Ti–B–C," *Ceram. Eng. Sci. Proc.*, **3**, 538–54 (1982).
[18]R. M. German, A. Bose, and N. S. Stoloff, "Powder Processing of High Temperature Aluminides," *Mater. Res. Soc. Symp. Proc.*, **133**, 403–14 (1989).
[19]G.Y. Richardson, R.W. Rice, W. J. McDonough, J. M. Kunetz, and T. Schroeter, "Hot Pressing of Ceramics Using Self-Propagating Synthesis," *Ceram. Eng. Sci. Proc.*, **7**, 761–70 (1986).
[20]J. B. Holt and Z. A. Munir, "Combustion Synthesis of Titanium Carbide: Theory and Experiment," *J. Mater. Sci.*, **21**, 251–59 (1986).
[21]M. A. Riley and A. Niiler, "Low Pressure Compaction of SHS Prepared Ceramics," Ballistics Research Laboratory Rept. No. BRL-MR-3574, Aberdeen Proving Ground, MD, March 1987.
[22]R.W. Rice, W. J. McDonough, G.Y. Richardson, J. M. Kunetz, and T. Schroeter, "Hot Rolling of Ceramics Using Self-Propagating High-Temperature Synthesis," *Ceram. Eng. Sci. Proc.*, **7**, 751–60 (1986).
[23]A. Niiler, L. J. Kecskes, T. Kottke, P. H. Netherwood, Jr., and R. F. Benck, "Explosive Consolidation of Combustion Synthesized Ceramics; TiC and TiB_2," Ballistics Research Laboratory Rep. No. BRL-TR-2951, Aberdeen Proving Ground, MD, December 1988.
[24]B. H. Rabin, G. E. Korth, and R. L. Williamson, "Fabrication of Titanium Carbide–Alumina Composites by Combustion Synthesis and Subsequent Dynamic Consolidation," *J. Am. Ceram. Soc.*, **73** [7] 2156–57 (1990).
[25]N. N. Thadhani: private communication.
[26]D. A. Hoke, M. A. Meyers, L.W. Meyer, and G.T. Gray III, *Metall. Trans.*, submitted for publication.
[27]L. E. Toth, *Transition Metal Carbides and Nitrides;* pp. 169–76. Academic Press, New York, 1971.
[28]G. Das, K. S. Mazdiyasni, and H. A. Lipsitt, "Mechanical Properties of Polycrystalline TiC," *J. Am. Ceram. Soc.*, **65** [2] 104–10 (1982).
[29]A. P. Katz, H. A. Lipsitt, T. Mah, and M. G. Mendiratta, "Mechanical Behavior of Polycrystalline TiC," *J. Mater. Sci.*, **18**, 1983–92 (1983).
[30]L. J. Kecskes and A. Niiler, "Impurities in the Combustion Synthesis of Titanium Carbide," *J. Am. Ceram. Soc.*, **72** [4] 655–61 (1989).
[31]D. B. Miracle and H. A. Lipsitt, "Mechanical Properties of Fine-Grained Substoichiometric Titanium Carbide," *J. Am. Ceram. Soc.*, **66** [8] 592–97 (1983).
[32]A. S. Rogachev, V. M. Shkiro, I. D. Chausskaya, and M.V. Shvetsov, "Gasless Combustion in the System Titanium–Carbon–Nickel," *Combust. Explos. Shock Waves (Engl. Transl.)*, **24** [6] 720–26 (1988).
[33]J. Wong, E. M. Larson, J. B. Holt, P. A. Waide, B. Rupp, and R. Frahm, "Time-Resolved X-ray Diffraction Study of Solid Combustion Reactions," *Science*, **249** 1406–409 (1990).
[34]M. A. Meyers and K. K. Chawla, *Mechanical Metallurgy: Principles and Applications;* p. 497. Prentice-Hall, Englewood Cliffs, NJ, 1984.
[35]E. Staskewitsch, *Fortschr.-Ber. VDI Z.*, **56**, 5 (1981).
[36]S. Kalpakjian, *Manufacturing Processes for Engineering Materials;* p. 275. Addison-Wesley, Amsterdam, Netherlands, 1984.
[37]P. Schwarzkopf and R. Kieffer, *Refractory Hard Metals: Borides, Carbides, Nitrides, and Silicides;* p. 72. Macmillan, New York, 1953.
[38]K. S. Vecchio, J. C. LaSalvia, and M. A. Meyers, *Metall. Trans.*, submitted for publication.
[39]M. Humenik, Jr., and N. M. Parikh, "Cermets: I, Fundamental Concepts Related to Microstructure and Physical Properties of Cermet Systems," *J. Am. Ceram. Soc.*, **39** [2] 60–63 (1956).
[40]A. K. Filonenko and V. I. Vershennikov, "Mechanism of Spin Burning of Titanium in Nitrogen," *Combust., Explos. Shock Waves (Engl. Transl.)*, **11** [3] 301–308 (1976).
[41]Y. M. Maksimov, A. T. Pak, G. B. Lavrenchuk, Y. S. Naiborodenko, and A. G. Merzhanov, "Spin Combustion of Gasless Systems," *Combust., Explos. Shock Waves (Engl. Transl.)*, **15** [4] 415–18 (1979).
[42]Y. M. Maksimov, A. G. Merzhanov, A. T. Pak, and M. N. Kuchkin, "Unstable Combustion Modes of Gasless Systems," *Combust., Explos. Shock Waves (Engl. Transl.)*, **17** [4] 393–400 (1981).
[43]A.V. Dvoryankin, A. G. Strunina, and A. G. Merzhanov, "Trends in the Spin Combustion of Thermites," *Combust., Explos. Shock Waves (Engl. Transl.)*, **18** [2] 134–39 (1982).
[44]A. G. Strunina, A.V. Dvoryankin, and A. G. Merzhanov, "Unstable Regimes of Thermite System Combustion," *Combust., Explos. Shock Waves (Engl. Transl.)*, **19** [2] 158–63 (1983).
[45]M. M. Carroll and A. C. Holt, "Static and Dynamic Pore-Collapse Relations for Ductile Porous Materials," *J. Appl. Phys.*, **43** [4] 1626–36 (1972).
[46]T. Altan, S. Oh, and H. L. Gegel, *Metal Forming: Fundamentals and Applications;* p. 128. American Society for Metals, Metals Park, OH, 1983.
[47]Y. G. Dorofeev and V.T. Prutsakov, "Energy Absorption during the Densification of Metal Powders at Loading Speeds of up to 50 m/s," *Sov. Powder Metall. Met. Ceram. (Engl. Transl.)*, **11** [3] 191–94 (1972).
[48]J. Puszynski, J. Degreve, and V. Hlavacek, "Modeling of Exothermic Solid–Solid Noncatalytic Reactions," *Ind. Eng. Chem. Res.*, **26** 1424–34 (1987).
[49]R.V. Voitovich and E. I. Golovko, *Poroshk. Metall.*, **183** [3] 55–61 (1978).
[50]B. L. Ferguson, A. Kuhn, O. D. Smith, and A. Hofstatter, "Hot Consolidation of Porous Preforms Using "Soft" Tooling"; in *Powder Metallurgy for Full Density Products,* New Perspectives in Powder Metallurgy: 8. Edited by K. M. Kulkarni. Metal Powder Industries Federation, Princeton, NJ, 1987. □